JOURNAL OF GUIDANCE, CONTROL, AND DYNAMICS
Vol. 32, No. 3, May–June 2009

Force–Stiffness Feedback in Uninhabited Aerial Vehicle Teleoperation with Time Delay

T. M. Lam,* M. Mulder,† M. M. van Paassen,‡ and J. A. Mulder§
Delft University of Technology, 2629 HS Delft, The Netherlands
and
F. C. T. van der Helm¶
Delft University of Technology, 2628 CD Delft, The Netherlands

DOI: 10.2514/1.40191

This study investigates the use of haptic feedback to support the teleoperation of an uninhabited aerial vehicle with time delay. Two means of supplying the haptic feedback are investigated: first, an additional force on the control inceptor, and second, an additional force combined with an increased stiffness of the control inceptor. The advantage of combining the force feedback with stiffness feedback, over force feedback alone, is that the additional stiffness of the control inceptor increases the authority of the haptic feedback system in critical situations. The goal of this study is to increase the safety of teleoperation while reducing operator workload. A theoretical analysis shows that force–stiffness feedback improves the stability in the human control loop while allowing for lower force-feedback gain settings as compared with force feedback alone, which indicates that this could contribute to reducing operator workload. In an experiment, the two haptic feedback conditions were compared with a baseline condition without haptic feedback. The fidelity of the experiment was improved over an earlier experiment by introducing a time penalty for collisions. The number of collisions was different for all three conditions, with the lowest number for the force–stiffness condition and the highest number for the baseline condition. Both haptic feedback conditions were rated equally on subjective workload metrics and scored better than the baseline. This finding is in contrast with results from earlier experiments, which indicated a higher workload with haptic feedback, and shows the importance of creating realistic test conditions when using subjective workload ratings.

Nomenclature

B	=	damping coefficient, N · m · s/rad
b	=	characteristic wave impedance, N · s/m
F	=	force, N
I	=	moment of inertia, kg · m^2
K	=	spring constant, N · m/rad
k	=	spring constant, N/m
M	=	moment, N · m
m	=	mass, kg
T	=	time, s
x	=	position, m
δ	=	stick deflection, rad
$\dot{\delta}$	=	stick deflection rate, rad/s
τ	=	time delay, s

Subscripts

c	=	commanded
ext	=	external
f	=	force
g	=	grip
h	=	hand
i	=	intrinsic
p	=	pitch, longitudinal
r	=	roll, lateral
s	=	stiffness
st	=	stick
tot	=	total

Received 1 August 2008; revision received 6 November 2008; accepted for publication 7 November 2008.

*Ph.D. Candidate, Control and Simulation Division, Faculty of Aerospace Engineering, Kluyverweg 1; t.m.lam@tudelft.nl.

†Associate Professor, Control and Simulation Division, Faculty of Aerospace Engineering, Kluyverweg 1; m.mulder@tudelft.nl. Member AIAA.

‡Associate Professor, Control and Simulation Division, Faculty of Aerospace Engineering, Kluyverweg 1; m.m.vanpaassen@tudelft.nl. Member AIAA.

§Professor, Control and Simulation Division, Faculty of Aerospace Engineering, Kluyverweg 1; j.a.mulder@tudelft.nl. Member AIAA.

¶Professor, Biomechanical Engineering Division, Faculty of Mechanical, Maritime and Materials Engineering, Mekelweg 2; f.c.t.vanderhelm@tudelft.nl.

I. Introduction

IN THE teleoperation of an uninhabited aerial vehicle (UAV), the operator is physically separated from the vehicle. Information for controlling the UAV, provided at the ground station, is usually visual. Images from cameras mounted on the vehicle are limited in resolution, dynamic range, and field of view. Teleoperators also lack other sensory information that pilots of a manned aircraft normally have, such as sounds, vibration, and physical motion. Additionally, the communication between the UAV and the ground station may have considerable time delays, for instance, when satellite communications are required. All these may contribute to poor situation awareness, poor efficiency, and potentially unsafe teleoperation [1–4].

To improve this situation, the operator will require information from sensors that can measure the distance to objects surrounding the UAV. Such information could be presented on a visual display; however, this would add to the already high workload on the operator's visual channel. Another option would be to add automation that modifies the operator's inputs to prevent collision. However, the drawback of this solution would be a decrease in situation awareness. The solution investigated here supports the human operator by means of haptic feedback, that is, through the sense of touch, on the control device. Previous studies have shown that haptic feedback can complement the visual information and increase teleoperation safety and efficiency [5–11]. For collision avoidance in UAV teleoperation, the focus of our study, Lam et al. [12] investigated the application of force offset, that is, the addition of an external force on the control device, in haptic feedback to assist operators in

controlling the UAV through an obstacle-laden environment. Virtual repulsive stick forces, generated by an artificial force field (or risk field) [13], are introduced on the control device. This provides operators with information about the environment and allows them to adapt their control input to avoid collisions. The effects of time delays, a well-known problem in teleoperation [2,14,15], were successfully countered by combining the force feedback with the wave variable transformation [16] developed by Niemeyer and Slotine [17,18]. All our investigations [12,16,19] showed that, with haptic feedback, the number of collisions decreased significantly, at the cost, however, of higher subjective workload ratings as compared with the situation without haptic feedback.

These higher ratings warrant an improved design and better tuning of the haptic feedback. In haptic feedback conditions, large variations in the force feedback and high stick deflection rates were found to contribute to physical workload, the dominant factor in the subjective ratings [12,16,19]. Although these effects could, in principle, be reduced quite easily, for example, by decreasing the force-feedback gain, this would make the haptic interface less effective, as the assisting forces become smaller. To overcome this problem, Abbink and Mulder [20] introduced the concept of "stiffness feedback," that is, changing the stiffness of the control device in conjunction with a well-tuned force feedback. This force–stiffness feedback was applied successfully in a haptic driver assistance system [21]. A first implementation of the novel feedback was tested in the context of UAV teleoperation, however, still without considering time delays in communication links and with a trial and error approach to the tuning [19]. Therefore, the first goal of this paper is to increase the safety of teleoperation and reduce operator workload by using a well-tuned combination of force feedback and stiffness feedback in UAV teleoperation with signal transmission time delays.

The higher workload ratings with haptic feedback might have been caused by something other than a nonoptimal tuning. In all our experiments conducted so far [12,16,19], the number of collisions indeed reduced considerably with haptic feedback (in some cases up to 80–90%), but workload still increased. Thus, although haptic feedback helped operators to significantly improve their performance, in their judgment of workload, the higher physical workload with haptic feedback dominated over all other workload causes. However, a common problem in these experiments was that there was no penalty at all when the UAV collided with an obstacle, a case that clearly does not approximate an operational setting. To increase the validity of the experiment, such a penalty was added by freezing the experiment for a minute every time a collision occurred. Hence, the second goal of this paper is to investigate whether introducing such a collision penalty would indeed lead to different subjective workload ratings as compared with the findings in our previous experiments [12,16,19].

This paper is structured as follows. The first part consists of a theoretical investigation of the use of combinations of force feedback and stiffness feedback. In Sec. II, four possible representations of haptic feedback are introduced. Because a haptic interface interacts with the operator through the neuromuscular system (NMS), a model of the NMS is described in Sec. III. This model is used in Sec. IV, in which the results of offline simulations that were conducted to tune the force feedback and force–stiffness feedback configurations for UAV collision avoidance are discussed. In the second part of this section, the force–stiffness feedback is evaluated in a human-in-the-loop experiment, introducing the penalty described earlier. The experiment is described in Sec. V. In Sec. VI, the results, focusing on the effectiveness of using force–stiffness feedback for UAV collision avoidance, regarding safety, performance, control activity, and workload are discussed. The paper ends with a discussion and final conclusions in Secs. VII and VIII, respectively.

II. Haptic Feedback Configurations

In this design of a haptic feedback system, we will explore haptic feedback by 1) increasing the force on the manipulator, 2) increasing the stiffness of the manipulator, and 3) two combinations thereof. Thus, four possible haptic feedback representations are discussed that all provide repulsive forces on a control device (here, a side stick) given a feedback variable that one wants to "display" through the device. Generally speaking, the haptic feedback has four requirements. First, in situations in which the operator removes his or her hand from the stick, the stick should actively deflect away from the direction of potential collisions, resulting in a safe evasive maneuver. Second, to increase the effectivity of the system, the feedback should be presented in such a way that operators are tempted to follow the force-feedback command as closely as possible. Third, the operator workload should be limited. Fourth, the safety of operation and operator performance should increase, leading to an increase in the number of successful teleoperation missions.

A. Force Feedback

In force feedback, a force offset F_f applied to the control manipulator is used to guide the operator. The total force that the operator perceives is the sum of the reaction force from the stick dynamics, F_{st}, and the external force offset. Assume that the stick is displaced to a certain position, x_{st}. Then the force exerted by the operator, that is, the force on the hand, F_h, is written as

$$F_h(x_{\text{st}}, i) = F_{\text{st}}(x_{\text{st}}) + F_f(i)$$
$$F_h(x_{\text{st}}, i) = k_{\text{st}} x_{\text{st}} + F_f(i) \tag{1}$$

Here $F_{\text{st}}(x_{\text{st}})$ is the force in the manipulator as function of the position, which, in this case, is defined by a constant spring constant, k_{st}. $F_f(i)$ the reaction force from the control device, which is a function of the haptic feedback information, i. Note that the stick deflection acts as the input to the system to be controlled, in this case, the UAV.

Figure 1 shows that, due to the haptic feedback force, the stick will have a nonzero neutral position (A), that is, the position at which the stick is in equilibrium in the absence of external forces. When the stick is released, $F_h(x_{\text{st}}, i) = 0$, due to the haptic feedback force the stick will *actively deflect*, resulting in $x_{\text{st}} = -F_f(i)/k_{\text{st}}$. This active deflection with hands off can be considered an "autonomous collision avoidance" function. In fact, the force feedback can be regarded as yielding a commanded stick deflection that the operator should follow as much as possible. That is, when yielding to the forces applied on the hand, the operator deflects the stick in a way that satisfies the collision avoidance function. Because a control device is typically limited in its deflections, there is a limit to the amplitude of the force feedback, resulting in a constraint on the force-feedback gain.

In previous studies, Lam et al. [12,16,19] found that the amplitudes of stick motions due to neutral position changes may contribute to workload. In particular, when flying through a narrow corridor or when moving along multiple smaller and closely spaced obstacles, the force offsets may vary continuously. If the operator is

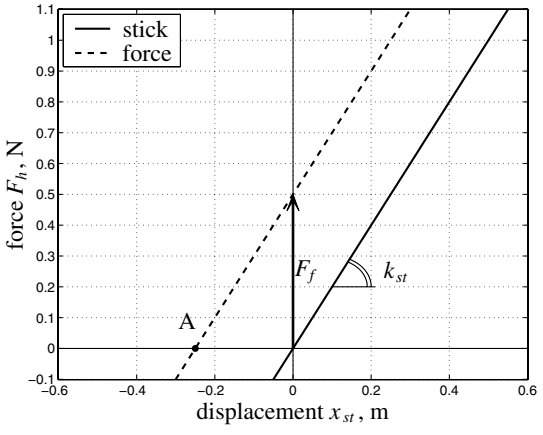

Fig. 1 Force-displacement relation of force feedback for a fixed *i*.

not able to follow the force feedback accurately, overshoots and control oscillations occur.

A possible solution would be to reduce the force offset magnitude, that is, decrease the force-feedback gain. This, however, may result in repulsive forces that are too small, in particular, for operators who adopt a high neuromuscular stiffness. It reduces the effectivity of the collision avoidance command function and limits the haptic presentation of information regarding a potential collision. Clearly, tuning the force-feedback magnitude needs a compromise between, on the one hand, the effectivity of the haptic interface and, on the other hand, the workload it imposes on the operator.

B. Stiffness Feedback

Stiffness feedback involves the addition of an extra spring load, $k_s(i)$, as function of haptic feedback information, i, to the nominal stick dynamics' spring constant, k_{st}. Instead of having a force offset, the stick becomes stiffer when in the presence of an obstacle, that is, the extra stiffness provides an impedance, resulting in an extra force that depends on the deflection of the stick by the operator. When the stick is released, it will *not actively deflect away* from a possible collision, as is the case when using force feedback, but it will return to the neutral position. Hence, stiffness feedback alone is not suitable for implementing autonomous collision avoidance. The total force that an operator perceives in this situation can be written as

$$\begin{aligned} F_h(x_{\mathrm{st}}, i) &= F_s(x_{\mathrm{st}}, i) + F_{\mathrm{st}}(x_{\mathrm{st}}) \\ F_h(x_{\mathrm{st}}, i) &= k_s(i)x_{\mathrm{st}} + k_{\mathrm{st}}x_{\mathrm{st}} \end{aligned} \tag{2}$$

where $F_s(x_{\mathrm{st}}, i)$ is the force due to an extra spring load $k_s(i)$. Figure 2 shows that the slope of the force-excursion relation increases due to the extra spring load. The line rotates around the origin; therefore, a zero displacement leads to zero repulsive force. Because small displacements result in relatively small repulsive forces, human operators may not even perceive sufficient information when using only small stick displacements. With a zero stick displacement, the operator will not be provided with any haptic feedback. In a case in which the UAV has moved very close to the obstacle, such as drift due to wind, the stiffness feedback would have become so large that the stick cannot be moved at all.

Clearly, providing only stiffness feedback is not a workable solution. The haptic device should be capable of actively deflecting the stick away from a possible collision, preferably with only a small overshoot from the zero displacement to not introduce control problems. It could be helpful, however, for the haptic device to be able to provide large resistance when the stick is deflected in the wrong direction, that is, with high risk of collision. Hence, when combining the force feedback with stiffness feedback, these two properties of haptic feedback can be achieved. Two possible combinations will be discussed next.

C. Stiffness–Force Feedback

The lack of active repulsive deflections of the control device with stiffness feedback can be resolved by combining it with force

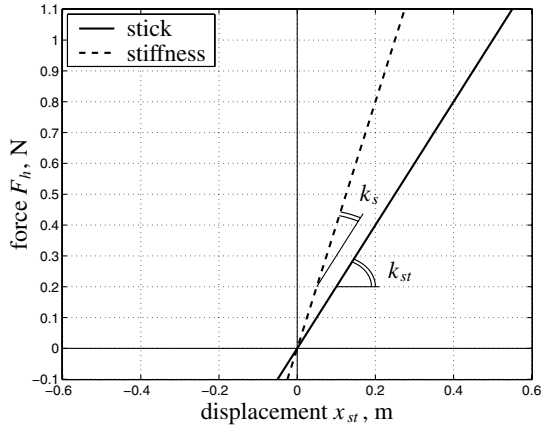

Fig. 2 Force-displacement relation of stiffness feedback for a fixed *i*.

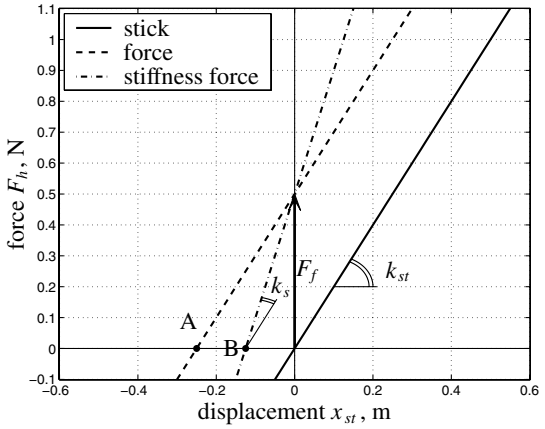

Fig. 3 Force-displacement relation of stiffness–force feedback for a fixed *i*.

feedback. The first possible combination, which is simply combining the force feedback and the stiffness feedback from previous sections, is referred to as stiffness–force feedback. In this case the total exerted force by the human operator is defined as

$$\begin{aligned} F_h(x_{\mathrm{st}}, i) &= F_{\mathrm{st}}(x_{\mathrm{st}}) + F_s(x_{\mathrm{st}}, i) + F_f(i) \\ F_h(x_{\mathrm{st}}, i) &= k_{\mathrm{st}}x_{\mathrm{st}} + k_s(i)x_{\mathrm{st}} + F_f(i) \end{aligned} \tag{3}$$

Figure 3 shows the force-excursion relation of the stiffness–force feedback, a haptic configuration that was tested by Lam et al. [19].

The drawback of this configuration is that, due to the increase in stiffness, the desired offset of the neutral position (A) commanded by the force feedback will decrease, which results in (B). In the hands-off case, $F_h(x_{\mathrm{st}}, i) = 0$, the stick deflection x_{st} becomes equal to $-F_f(i)/(k_{\mathrm{st}} + k_s(i))$, that is, the stiffness feedback actually *reduces* the effects of the force feedback. Although this may have a positive effect on operator workload, as was indeed reported by Lam et al. [19], a reduction of the force offset inevitably leads to a less-effective collision avoidance. As a matter of fact, the number of collisions found by Lam et al. [19] was, albeit not significantly, considerably larger with the stiffness–force feedback than with force feedback alone.

D. Force–Stiffness Feedback

From the aforementioned findings, it is clear that the desired property of force feedback, that is, a nonzero neutral position shift that, in the hands-off situation, actively deflects the stick away to avoid a possible collision, must be maintained. To this end, the offset force should be *compensated* for the additional stiffness introduced by the stiffness feedback, as was first proposed by Abbink and Mulder [20]. The result is a configuration with the same neutral point shift as the force feedback, but in which the stiffness also varies with force feedback. Deviations from the "commanded" force are communicated through the stiffness feedback, motivating the operator to more accurately follow up on it. In the following, this combination of force and stiffness feedback will be referred to as force–stiffness feedback. The total exerted force can be written as

$$F_h(x_{\mathrm{st}}, i) = F_{\mathrm{st}}(x_{\mathrm{st}}) + (F_s(x_{\mathrm{st}}, i) + F'_s(i)) + F_f(i) \tag{4}$$

where $F'_s(i)$ represents the extra force offset needed to account for the effect of stiffness feedback to maintain the same neutral position offset (A). Figure 4 illustrates that this extra force offset can be calculated using the force feedback $F_f(i)$, the extra spring load $k_s(i)$, and the control device spring constant k_{st}:$F'_s(i) = (k_s(i)/k_{\mathrm{st}})F_f(i)$. In the hands-off situation, the active stick deflection remains $-F_f(i)/k_{\mathrm{st}}$.

The force–stiffness feedback configuration combines the best of both options: the force feedback actively guides the UAV away from a possible danger and the *stiffness feedback informs operators about undesired stick deflections and restricts them from deviating the stick too much from the guidance provided by the force feedback*. The

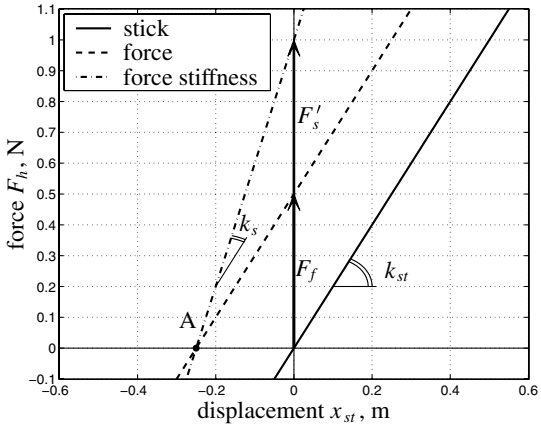

Fig. 4 Force-displacement relation of force–stiffness feedback for a fixed *i*.

stiffness feedback can be considered as a haptic display that informs the operator of the urgency of the situation. When the gain of the stiffness feedback increases, the operator is less able to overrule the haptic feedback and the system becomes more and more autonomous [20].

When considering this property of force–stiffness feedback from another perspective, making the force feedback more compulsive would, in principle, allow for lower force-feedback gains. Because the force feedback adds to the physical workload, as concluded from previous experiments [12,16,19], this may yield a lower operator workload. With force feedback alone, reducing the force-feedback gain would result in smaller repulsive forces, rendering the haptic system less effective. However, the addition of stiffness restores the authority of the haptic feedback, enabling effective haptic feedback at a lower force-feedback gain. Hence, this system is hypothesized to further improve haptic feedback for collision avoidance in UAV teleoperation while reducing workload and improving acceptance.

Before evaluating the force–stiffness feedback configuration in a human-in-the-loop experiment, the main characteristics of the novel feedback will be investigated and the tuning will be verified using offline computer simulations. In these simulations, a model of the human teleoperator is needed and, because operators interact with the haptic interface via their neuromuscular system, a model of the human NMS is first described.

III. Neuromuscular Model

The haptic side stick used in this study has two axes, roll (left/right) and pitch (forward/backward). As only the planar, horizontal movements of the UAV are considered, the repulsive forces by haptic feedback result in stick motions in two dimensions.

A. Force, Position, and Relax Tasks

With an operator holding the stick, the effects of haptic feedback depend on the NMS dynamics of the arm and hand, which may include adaptive reflexive behavior [22,23]. For instance, the neuromuscular stiffness is not fixed, but changes due to the settings of the reflexive feedback gains, the characteristics of which in turn depend on, among others, the bandwidth of external disturbances on the control device.

The NMS dynamics also depend on the task. When it is desirable that the operator follow the movement of the control device, it is required that the exerted force on the device is kept constant. This is called a force task, and the operator will select a setting for the NMS that will produce a large endpoint admittance. When it is desirable to keep the position of the control device constant, suppressing external disturbances, the NMS has a low endpoint admittance and the task is referred to as a position task. Between the force and position tasks, one can identify the relax task, in which reflexive feedback is suppressed. In that case, reflexes play no role and the intrinsic properties of the muscle and limb define the NMS dynamics.

The adaptive, reflexive behavior of the NMS makes it difficult to find an optimal setting for the haptic interface. For each setting, the operator consciously or subconsciously adapts the NMS characteristics to perform well. The design point for the haptic feedback is chosen to match the NMS model *without* reflexive feedback, that is, as measured in the relax task. The rationale of this choice is that, for a relax task, the reflexes play no role and the physical work of the operator is minimal.

B. Neuromuscular System Model

Figure 5 shows a schematic representation of the NMS model used in this study. The model contains activation dynamics, force feedback from the Golgi tendon organs (GTO), arm inertia, intrinsic muscle damping and stiffness, reflexive feedback of the muscle length and velocity from the muscle spindles, and grip dynamics.

The GTO and muscle spindle feedback enable an operator to modify the effective properties (impedance) of the limb. This makes the performance of the combined system insensitive to the tuning of the force and stiffness feedback; if a nonoptimal tuning is applied, the human operator will correct for this by selecting a different impedance for the neuromuscular system. However, a nonoptimal setting will have a negative influence on operator workload and comfort. For the gains for the force and stiffness feedback system, we therefore aim to design for a condition in which the operator does not need the reflexive feedback paths. This corresponds to the neuromuscular system properties as measured in a relax task.

In that case, both the GTO force feedback as well as the reflexive feedback of the muscle spindles can be neglected and, as a consequence, the gains K_f, K_v, and K_p are all assumed to be zero. The remaining parameters for the arm intrinsic properties and the grip dynamics were identified for a two-dimensional NMS model [24], using the two-axis side stick as used by Lam et al. [12,19,25], the same stick that is used here. The NMS parameters adopted here correspond to those obtained for a representative subject.

The activation dynamics generate muscle forces based on the activation signal U that originates from the human cognitive control behavior, in this study the primary feedback based on what the operator perceives visually from the environment. Activation dynamics are modeled by a second-order system [22,26,27], with a natural frequency of $\omega_o = 2\pi f_a$ ($f_a = 2.2$ Hz [22]) and a damping of $\beta = \sqrt{2}/2$.

The inertia matrix I_i in Newton meter second squared per radian, the damping coefficient matrix B_i in Newton meter second per radian, and the spring constant matrix K_i in Newton meters per radian are

$$I_i = \begin{bmatrix} I_{i_{rr}} & I_{i_{rp}} \\ I_{i_{pr}} & I_{i_{pp}} \end{bmatrix} = \begin{bmatrix} 0.0077 & 0.0003 \\ 0.0003 & 0.0147 \end{bmatrix} \tag{5}$$

$$B_i = \begin{bmatrix} B_{i_{rr}} & B_{i_{rp}} \\ B_{i_{pr}} & B_{i_{pp}} \end{bmatrix} = \begin{bmatrix} 0.0574 & 0.0277 \\ 0.0277 & 0.5052 \end{bmatrix} \tag{6}$$

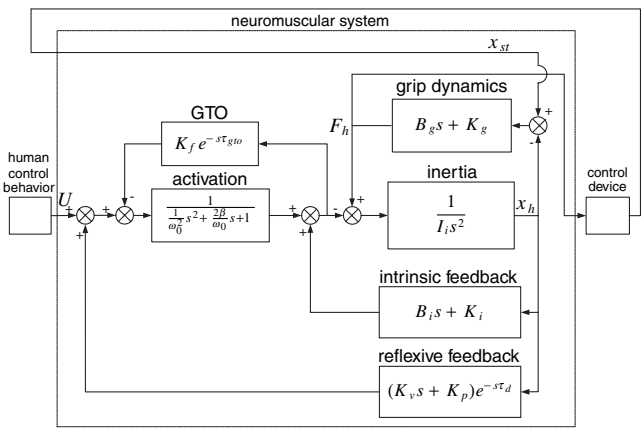

Fig. 5 Model of the human neuromuscular arm interacting with environment, adopted from De Vlugt [23].

and

$$K_i = \begin{bmatrix} K_{i_{rr}} & K_{i_{rp}} \\ K_{i_{pr}} & K_{i_{pp}} \end{bmatrix} = \begin{bmatrix} 1.2050 & -0.8436 \\ -0.8436 & 9.2034 \end{bmatrix} \quad (7)$$

These matrices describe the two-dimensional intrinsic properties of the NMS; the subscripts r and p represent the lateral (roll) and longitudinal (pitch) directions, respectively.

The diagonal elements in the NMS model show larger inertia, viscosity, and stiffness properties in the longitudinal direction as compared with the lateral direction. This indicates that, with this particular control device, the operator can provide more resistance to disturbances in the pitch than in the roll. Moreover, the NMS principal axes do not necessarily align with those of the control device and, as a result, the lateral and longitudinal NMS dynamics, when defined in the control device reference frame such as here, are coupled. For example, in K_i the negative value for $K_{i_{rp}}$ indicates that a negative displacement in the pitch direction contributes to the stiffness in the roll direction.

A rotation of the side-stick axes could remove this cross coupling; however, this rotation would have to be defined and changed for each subject individually. It was chosen here to keep the stick axes' orientation fixed, although it is recommended for a final design that an optimal orientation for the stick axes is investigated.

The effects of the tissue between the hand (position x_h) and the control device (position x_{st}) are modeled by the grip dynamics that yield an exerted force on the hand, F_h. The damping coefficient matrix B_g in Newton meter second per radian and the spring constant matrix K_g in Newton meters per radian are

$$B_g = \begin{bmatrix} B_{g_{rr}} & B_{g_{rp}} \\ B_{g_{pr}} & B_{g_{pp}} \end{bmatrix} = \begin{bmatrix} 2.0268 & 0 \\ 0 & 2.5046 \end{bmatrix} \quad (8)$$

and

$$K_g = \begin{bmatrix} K_{g_{rr}} & K_{g_{rp}} \\ K_{g_{pr}} & K_{g_{pp}} \end{bmatrix} = \begin{bmatrix} 163.2491 & 0 \\ 0 & 298.4789 \end{bmatrix} \quad (9)$$

This NMS model will be used in the offline simulations discussed in Sec. IV.

IV. Offline Simulations

The haptic feedback is based on the force field elaborated by and studied in Boschloo et al. [13]. In that study, the feedback from the force field was added directly to the control input of the UAV. Here, a model of the NMS is used to study the differences between force feedback and force–stiffness feedback using two kinds of simulations. First, a step response of the closed-loop system will be analyzed, with the vehicle position used for haptic feedback. Second, a UAV teleoperation simulation will be described, using a representative artificial force field to generate haptic feedback for collision avoidance [19].

A. Step Response

To illustrate the effect of using an extra spring load in a force–stiffness feedback system, a step response of the closed-loop operator/UAV system along 1 degree of freedom is investigated. A unit step input ($U = 1$) is applied to the neuromuscular activation dynamics, representing a voluntary input by an operator.

Figure 6a shows a schematic representation of the closed-loop system; Fig. 6b zooms in on the haptic interface implementation. The vehicle dynamics response, H_{UAV}, is modeled with the transfer function $2/(s+2)$ between the stick displacement, x_{st}, representing a velocity command, and the UAV velocity. The UAV lateral position, x, is used for haptic feedback. For force feedback, the feedback gains are $G_f = 4$ N/m and $G_s = 0$ N/m^2; for force–stiffness feedback, the gains are $G_f = 4$ N/m and $G_s = 4$ N/m^2.

The step response (Fig. 7) shows that, when using force–stiffness feedback, the vehicle steady-state position deviation is smaller and has less oscillations. Likewise, the stick displacement has less oscillations and smaller amplitudes (Fig. 7b). These results illustrate the property of force–stiffness feedback, that is, with increasing stiffness it reduces the ability of the human operator to (inadvertently) control the UAV away from the optimal path [20].

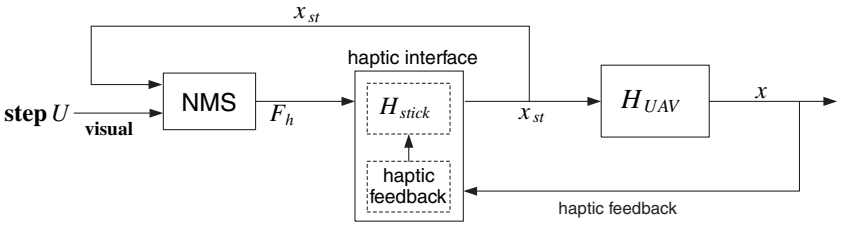

a) Closed-loop operator/vehicle system with UAV position x serving as haptic feedback information and x_{st} representing stick deflection. U and F_h are visual step input and hand force, respectively

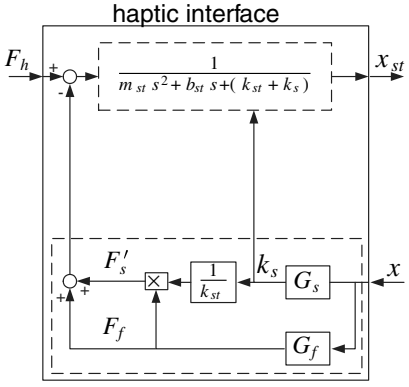

b) The haptic interface in detail with F_h and x_{st} serving as input and output of the control device, respectively. The UAV position x serves as input to the haptic interface

Fig. 6 Scheme of the operator/vehicle system and the haptic interface.

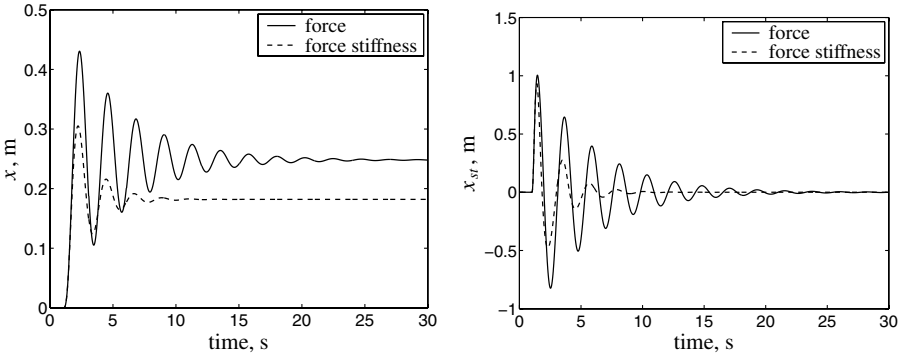

a) UAV position, x **b) Stick displacement, x_{st}**

Fig. 7 Step response of the vehicle position and stick displacement.

B. UAV Teleoperation

With force–stiffness feedback, the operator is expected to be better able to follow the haptic feedback information. It is important, however, that the guidance provided by the force feedback is well tuned. This means that the performance of the joint system must be acceptable and that the setting of the operator's NMS reflexes must be a comfortable one. This subsection describes computer simulations that show the application of force–stiffness feedback in UAV teleoperation. The settings for the relax task are used here for the NMS. The simulations should demonstrate that gains for the haptic force and stiffness feedback lead to acceptable joint system performance.

1. *Setup of the Closed-Loop Operator/UAV System*

Figure 8 shows a schematic representation of the closed-loop model. The model contains an operator model with a neuromuscular system, a stick control device, a UAV, and an artificial force field. The components of the model will be described in more detail next.

The human operator is modeled as a proportional controller, acting on the position error (gain P1) and heading error (gain P2) with respect to a fixed two-dimensional target position. The output of the pilot, U, will activate the neuromuscular system to exert a moment input, M_c, on the haptic control device, a two-axis side stick.

The stick, H_{stick}, is modeled as a mass-spring-damper system that has identical properties in the lateral and longitudinal directions with a moment of inertia of $I_{\text{st}} = 0.01\ \text{kg} \cdot \text{m}^2$, a damping coefficient of $B_{\text{st}} = 0.2\ \text{N} \cdot \text{m} \cdot \text{s/rad}$, and a spring constant of $K_{\text{st}} = 2\ \text{N} \cdot \text{m/rad}$. (Note that here the human–stick interaction is defined using moments and rotations rather than forces and displacements.) The stick deflection, δ_c, serves as a rate command for the UAV model. Maximum stick deflections, $\delta_{\max}$, are ± 0.35 and ± 0.40 rad in the longitudinal and lateral directions, respectively.

The UAV, H_{UAV}, is assumed to be a control-augmented helicopter [28]. A longitudinal stick deflection represents a velocity command in the longitudinal direction, with second-order dynamics, $1/((0.3s + 1)(0.18s + 1))$. A lateral stick deflection represents a yaw-rate command with first-order dynamics, $1/(0.2s + 1)$. The UAV has a maximum velocity of $5\ \text{m/s}$ and a maximum acceleration of $1\ \text{m/s}^2$.

The artificial force field (AFF) is used to map obstacles to repulsive forces. An integrated sensor is simulated that is able to do a 360 deg scan of the environment, with an angular resolution of 3 deg [29]. The sensor range is 50 m. The repulsive force vectors, generated by the AFF, point along the sensor radial lines. The parametric risk field from Lam et al. [29] is used, with parameters of $d_{\min} = 1.5$ m and $t_{\text{ahead}} = 2$ s. (For a detailed description of this AFF and its parameters, the reader is referred to Lam et al. [29].) The AFF output in both the longitudinal and lateral directions is a dimensionless risk value, ranging between 0 (no risk) and 1 (highest risk), which is converted to a force offset and extra spring load using gains G_f and G_s, respectively.

The control input and haptic feedback are subjected to a fixed transmission time delay of $\tau = 0.2$ s, simulating a satellite communication link between the UAV and ground control station. For haptic feedback, wave variables are used with wave impedance, $b = 0.3\ \text{N} \cdot \text{s/m}$, to reduce time delay effects [16,30]. The visual feedback (x, y, and ψ) is subjected to the same time delay; as customary, no wave variables are applied here.

2. *Haptic Feedback Configurations*

Three conditions are evaluated. First, force feedback with $G_f = 1.5\ \text{N} \cdot \text{m}$ is simulated, a representative case when considering an operator's exerted moment, pushing the stick to the limited deflection. With the spring constant K_{st} set at $2\ \text{N} \cdot \text{m/rad}$, the maximum repulsive force of $1.5\ \text{N} \cdot \text{m}$ results in a maximum neutral position change of 0.75 rad, which exceeds the deflection limits, $\delta_{\max}$, in both directions.

Assuming that physical load is contributed by large neutral position changes, a straightforward solution would be to reduce force feedback. With reduced force feedback, $G_f = 0.45\ \text{N} \cdot \text{m}$ (a reduction to 30%), our second condition, the maximum neutral position change would be 0.225 rad, which is still within the deflection limitations. It is questionable, however, whether the reduced force feedback will be sufficient to control the UAV through various environments without collision.

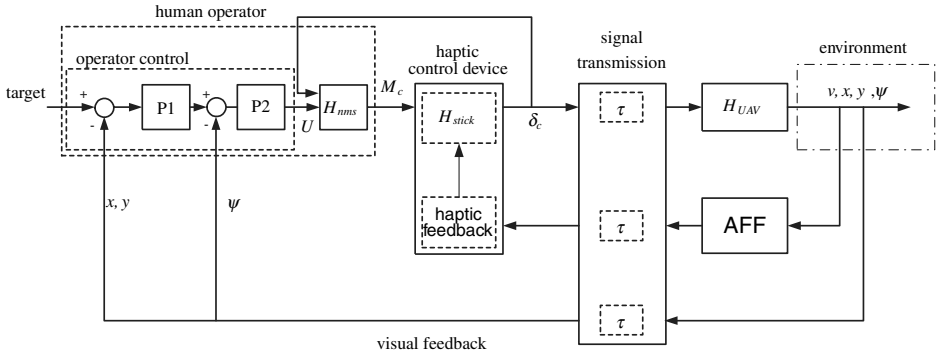

Fig. 8 Schematic representation of the closed-loop operator/UAV system with haptic feedback.

The third condition involves force–stiffness feedback, augmenting the reduced force feedback with stiffness feedback. Note that when G_s is set to $1.5/\delta_{\max}$ N · m/rad in the force–stiffness feedback condition, the maximum repulsive force generated by the extra spring load with maximum deflection, $\delta_{\max}$, would be 1.5 N · m. With the addition of the reduced force offset, the total repulsive force with force–stiffness feedback will then be larger than 1.5 N · m, the maximum value of force feedback alone. This requires the stick to be fully deflected with maximum risk value; however, this is something that will only very rarely occur as operators will use smaller deflections and the UAV velocity will decrease (smaller size of AFF) when haptic feedback is active and perceived.

The stiffness gains G_{sr} and G_{sp} for the force–stiffness feedback are tuned to each of the trajectories. This resulted in the values given in the right half of Table 1. The left part of this table shows the gains for the pilot model used. These were tuned to the trajectory and kept constant for all haptic feedback conditions.

3. Environment

The same trajectories were used as in Lam et al. [19]; they are shown in Fig. 9. The start and target positions are represented by the circle and star symbols, respectively. The dashed circles indicate the UAV position, whereas the arrows show the magnitudes and directions of the repulsive forces, all with a 1 s interval. Representative maneuvers, such as making a sharp turn (A), a passage through a narrow corridor (B), stopping before a dead-end (C), and moving through a passage with irregularities in the wall (D), were used to test the effectiveness of the three haptic feedback configurations.

4. Results and Discussion

Figure 9a illustrates that, with force feedback alone, our baseline, the UAV reaches all targets without collisions. The reduced force-feedback condition leads to collisions in trajectories B, C, and D; see Fig. 9b, indicating that, apparently, the feedback provided is insufficient to safely guide the UAV through these scenarios. When adding stiffness feedback to the reduced force feedback, the UAV is once again able to safely move through the environment; see Fig. 9c.

In the simulations, the operator model is a simple proportional controller [31] with the UAV position and heading errors as inputs. For this comparison, the gains for this controller were taken as equal for the three haptic feedback conditions. The pilot does not have any visual feedback of the environment constraints, however, and "blindly" flies toward the target. For collision avoidance, the model fully relies on the guidance provided by the haptic feedback. It is clear that the reduced force feedback alone is insufficient for collision avoidance, but that the reduced feedback in combination with the stiffness feedback performs as well as the base condition.

In reality, operators are provided with limited visual information about the environment constraints, and combine the visual and haptic information to determine an appropriate control signal. Reduced force feedback would lead to the perception of small forces or no perception of forces at all, and operators may dominantly rely on the visual information. Then again, a high risk of collision still exists, as the visual information, often provided by cameras mounted on the vehicle, is limited in field of view and resolution.

Force–stiffness feedback enables smaller force-feedback gains, that is, smaller force offsets, while still providing sufficient repulsive force magnitudes due to the addition of extra spring load. Smaller force offsets are desired in a flight through a narrow corridor or between closely spaced obstacles (e.g., trajectory B). The resulting stick deflections are large enough to avoid collision with an obstacle, as the stiffness feedback drives the operator to more consistently yield to the force-feedback command, and limits overshoots that may lead to collisions with obstacles during the avoidance maneuver. Based on the outcomes of our previous experiments [12,16,25], this may all be expected to result in lower operator workload. It can be concluded that force–stiffness feedback with small force-feedback gain can yield the same performance as with force feedback alone, without suffering from poor perception of repulsive forces.

Note, however, that although the force offset changes may be lower with force–stiffness feedback, the perceived repulsive forces that are partly caused by the addition of stiffness feedback may also be experienced as too large, again contributing to workload. In fact, with very high stiffness-feedback gains the operator has no alternative but to rapidly follow the commands generated by the force feedback. Obviously, the proper tuning of the force feedback and stiffness-feedback gains needs to be evaluated using a human-in-the-loop experiment, the subject of the remainder of this paper. As a basis for the tuning in that experiment, the stiffness values optimized for trajectory D were chosen, because it is expected that these will result in a relatively mild haptic feedback that would function well enough, considering that human subjects, unlike the model here, would plan conflict-free paths.

V. Experiment

An experiment was conducted to investigate the effects of using force–stiffness feedback as an alternative to haptic feedback based on force offsets alone in UAV teleoperation. The investigation focused on collision avoidance effectiveness, operator performance, control activity, and workload. The experiment setup was similar to the ones used and reported in earlier studies [12,16,19].

One aspect of the setup was changed, however. In the cited studies, experimental subjects could continue their flight in spite of a collision and were not provided with any information about whether or not a collision had occurred. As recommended by Lam et al. [16], it would be interesting to investigate the effects of introducing a penalty for collisions, for instance, by pausing the experiment for a few minutes every time a collision occurred. Tentatively, this could result in more frustration on the part of the operators, increasing their workload, in particular, for the configurations in which collisions are likely to occur. It will also force operators to act more cautiously. It can be hypothesized that operators become more appreciative of the haptic feedback when it helps them to prevent collisions and allows them to perform their task quicker. Therefore, in the current experiment a penalty for each collision was given, as will be elaborated.

A. Method

1. Subjects and Instructions to Subjects

Eleven subjects, aged between 23 and 27 years, with no previous flight experience, participated in the experiment. A reconnaissance

Table 1 Operator model proportional gains, force–stiffness feedback force gains, and optimized stiffness gains, where subscripts *p* and *r* represent the roll and pitch directions, respectively

Trajectory	Visual feedback		Force–stiffness feedback			
			Lateral		Longitudinal	
	P1, rad/m	P2	$G^*_{f_r}$, N · m	$G^*_{s_r}$, N · m/rad	$G^*_{f_p}$, N · m	$G^*_{s_p}$, N · m/rad
A	0.09	2.3	0.45	6.38	0.45	7.29
B	0.05	1.7	0.45	15.00	0.45	17.14
C	0.02	9.0	0.45	——[a]	0.45	4.71
D	0.02	0.9	0.45	3.38	0.45	4.29

[a]Omitted, because case C is symmetric.

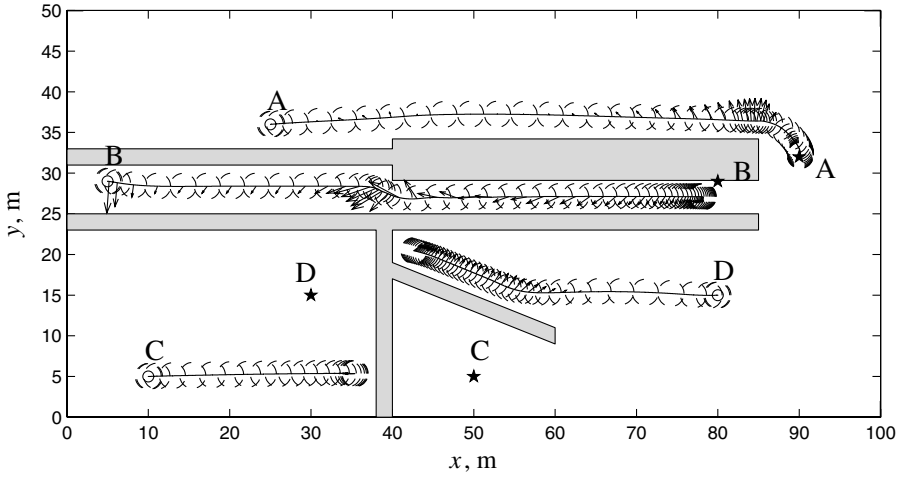

a) Force feedback

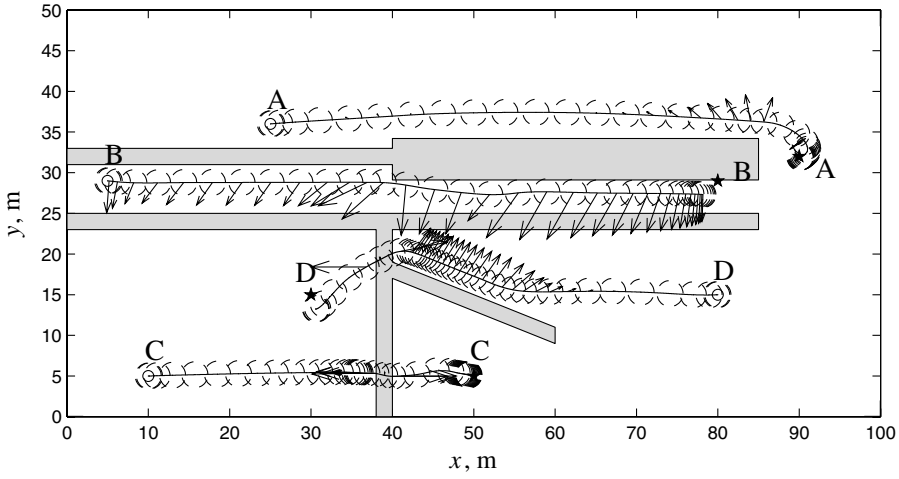

b) Reduced force feedback

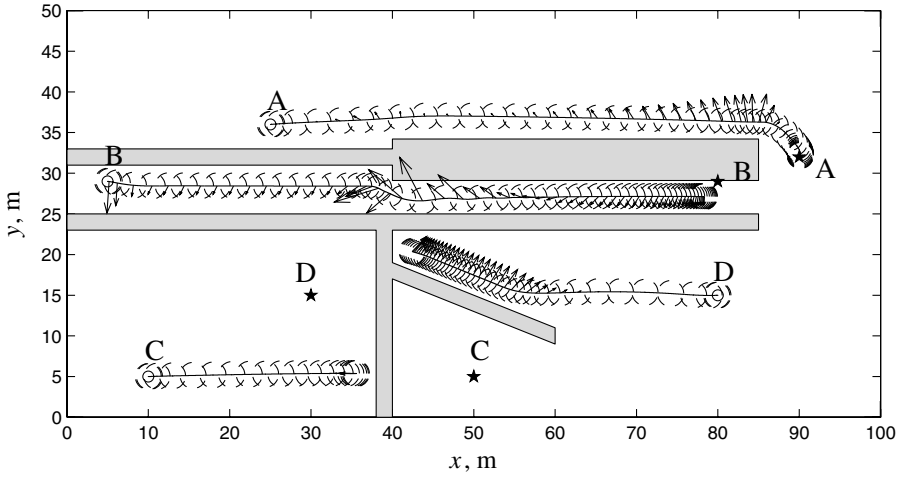

c) Force-stiffness feedback

Fig. 9 Simulation results of the closed-loop operator/UAV system.

or surveillance task in a hazardous environment was simulated. The subjects' main task was to fly a UAV through an environment with various buildings from waypoint to waypoint. They were instructed to fly as fast as possible and to aim for flying through the center of each waypoint as accurately as they could, but to avoid collisions.

The waypoints were marked by smoke plumes located in the vicinity of the buildings. When a collision occurred, subjects were notified by a loud beep and were given a penalty of 60 s, during which they could not fly. After the 60 s, the UAV was reset to the reset initial position as defined in Sec. V.A.4.

After each run, subjects were asked to rate their workload using the NASA Task Load Index (TLX) rating scale [32]. The TLX assumes that operator workload is caused by six sources: mental load, physical load, temporal load, performance, effort, and frustration level. First, subjects needed to choose from each paired combination (15 in total) of the six sources which one contributed most to their workload, yielding the TLX weights. Second, each source was given a rating using a scale ranging from low to high (except for the performance, which was rated using a scale ranging from good to bad), yielding the TLX

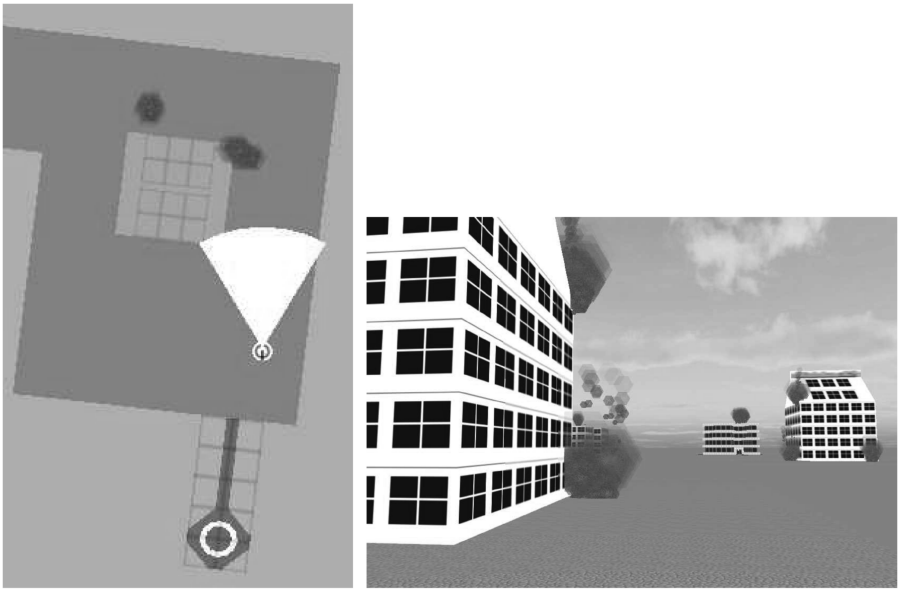

a) 2-dimensional navigation display **b) 3-dimensional camera display**

Fig. 10 Navigation and camera display.

ratings. The total TLX workload is then computed as per the procedure in [32].

2. Apparatus

The experiment was conducted in a fixed-base flight simulator. Subjects were seated on an aircraft chair in front of an 18 in. screen projecting a navigation display, as shown in Fig. 10a. The image from a simulated onboard camera, as shown in Fig. 10b, was projected on a wall at a distance of 2.9 m from the operator. The width and height of the projected image were 1.05 and 0.75 m, respectively, resulting in a field of view of 20 deg horizontally and 15 deg vertically. The display presented a camera view of with a field of view of 60 by 45 deg.

On the right-hand side of the chair, an electrohydraulic side stick was mounted, which was used as the haptic control device. Linear mass-spring-damper dynamics were simulated with an inertia of $I_{\text{st}} = 0.01\ \text{kg} \cdot \text{m}^2$, a damping coefficient of $B_{\text{st}} = 0.2\ \text{N} \cdot \text{m} \cdot \text{s/rad}$, and a spring constant of $K_{\text{st}} = 2\ \text{N} \cdot \text{m/rad}$. The position of the hand contact point was located at approximately 0.09 m above the axes of rotation. Identical stick dynamics were simulated in the pitch and roll axes; maximum deflections were 0.40 and 0.35 rad, respectively.

Both the visual and haptic channels had a fixed time delay of $\tau = 0.2$ s, simulating a delayed communication link between the UAV and the operator ground control station. Note that both the side-stick settings as well as the time delay used were the same as in the offline simulations discussed in Sec. IV.B.

3. UAV Model

A control-augmented UAV helicopter model was used, with identical dynamics as used in the offline simulations discussed in Sec. IV.B. A longitudinal stick deflection represented a velocity command V_x whereas a lateral stick deflection generated a yaw-rate rotation along the z axis $\dot{\psi}$, both with respect to a rotating Geodetic axis system (Fig. 11).

The helicopter model had a maximum velocity of 5 m/s and a maximum acceleration of 1 m/s^2. The altitude was automatically kept constant at 3.5 m. The UAV had a circular protection zone with a radius of 1.6 m. The intersection of any object with this zone was considered a collision and caused the simulation to freeze for 60 s.

4. Independent Variables

Two independent variables were defined.

First, there were three control configurations (CF): 1) no haptic feedback (NF), the baseline condition; 2) force feedback (FF) with $G_{f_r} = G_{f_p} = 1.5\ \text{N} \cdot \text{m}$ and wave variables ($b = 0.3\ \text{N} \cdot \text{s/m}$); and 3) force–stiffness feedback (FSF) with $G_{f_r} = G_{f_p} = 0.45\ \text{N} \cdot \text{m}$, $G_{s_r} = 3.75\ \text{N} \cdot \text{m/rad}$, $G_{s_p} = 4.29\ \text{N} \cdot \text{m/rad}$ and wave variables $b = 0.3\ \text{N} \cdot \text{s/m}$

These settings were the same as used in the full-force feedback and reduced-force feedback with stiffness-feedback conditions reported in Sec. IV for trajectory D.

Second, six subtasks (ST) were defined that involved different scenarios, each requiring a specific maneuver that may lead to control difficulties; they are illustrated in Fig. 12. Here, an arrow shows the flight direction starting from the reset initial position. When a collision occurred, the UAV was positioned and oriented at this location. The stars indicate the locations of smoke plumes, which in some cases doubled as waypoints. The secondary purpose of the smoke was to reduce the visibility of the boundaries of obstacles located in the vicinity.

1) In this subtask, the helicopter had to round the corner of a building, making a 90 deg turn (Fig. 12a). Before the turn, the UAV had to approach the first waypoint, forcing the UAV to fly closely along the corner. The second waypoint was located closely after the corner, to motivate subjects to make as sharp a turn as possible.

2) Here, the helicopter was to fly through a narrow gate with the pillars serving as two closely spaced, small obstacles. Figure 12b shows a cross section of the gate. The three smoke locations reduced the visibility of the passage and the pillar boundaries, making it more difficult to fly through the gate. The smoke plumes did not serve as waypoints in this subtask.

3) This subtask demanded a special task during hover. Once the UAV reached the diamond, it was supposed to rotate to the right and then move *backward* toward the building until the operator could see

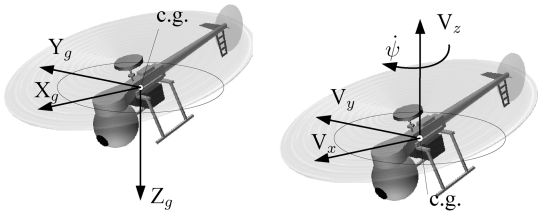

a) Rotating geodetic axis frame **b) Helicopter commands**

Fig. 11 Reference frame of the UAV model.

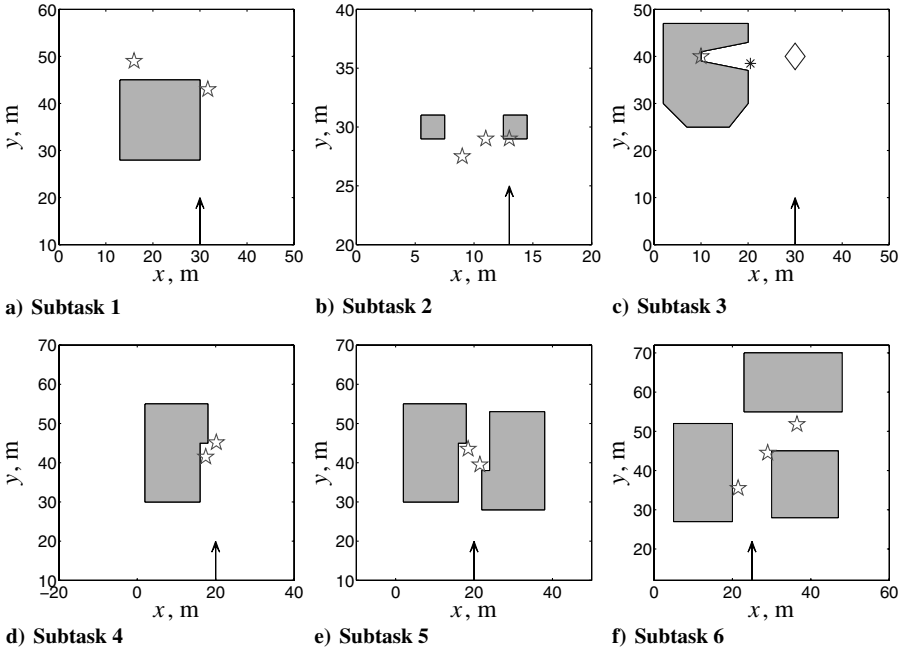

Fig. 12 Six subtasks used in the experiment.

a stop sign that was located below the UAV and fixed in the world (at the asterisk), as shown in Fig. 12c. During this maneuver, the camera did not point in the direction of motion and it was expected that haptic feedback would become very useful. Smoke appearing from the top of the building reduced the visibility of the building edges. Again, the smoke plume did not serve as a waypoint.

4) This scenario consisted of a building with a discrete change in the shape of the wall. The first waypoint was located before this change and would force the UAV to approach the wall, followed by an escape maneuver to avoid collision with the extension of the wall (Fig. 12d). The second waypoint was placed to force the UAV to stay close to the building during the escape maneuver.

5) Two buildings with discrete changes in opposite directions could lead to stick oscillations and considerable control difficulties. The first waypoint, located on the right, would force the UAV to make a sharp turn, whereas the second waypoint, located on the left, would force the UAV to make an escape maneuver (Fig. 12e).

6) In this subtask, the turn radius with haptic feedback would be limited due to the obstacles in front and on the left-hand side. It was expected that this subtask would lead to control difficulties when approached with a high velocity. The first waypoint on the left would force the UAV to approach the side of the left building, whereas the second waypoint would force the UAV to make a quick turn to fly closely along the corner of the right building. The third waypoint forced the UAV to approach another wall after the turn (Fig. 12f).

5. *Trajectory*

The trajectories (scenarios) were the same as those used by Lam et al. [12,16,19]. To simplify navigation, the subtask areas were marked with a darker background color on the navigation display (Fig. 10a). To prevent boredom, six trajectories were designed, each containing three different sectors [12]. In turn, each sector contained the six subtasks in a randomized order.

Table 2 shows the sectors and the corresponding subtask order. A trajectory contained three repetitions of each subtask and was flown once for each of the three control configurations. Each subject flew $3 \times 6 = 18$ runs. A typical run, without collisions, lasted approximately 6 min. An example trajectory can be found in earlier publications by Lam et al. [12,16].

6. *Experiment Procedure*

Before the actual experiment, the subjects familiarized themselves with the three control configurations in several training runs. Then, each subject flew the 18 experiment runs in one of three randomized orders. Subjects were not informed beforehand about what control configuration they flew during the measurement runs.

7. *Dependent Measures*

Control activity was represented by the standard deviation and the mean of the total exerted moment by the hand ($\sigma_{M_h}, \bar{M}_h$) and the standard deviation of the stick deflection rate ($\sigma_{\dot{\delta}_{\text{tot}}}$). (Here, total refers to the fact that the stick roll and pitch dimensions were summed vectorially.) Haptic activity was represented by the standard deviation and the mean of the total external moment exerted by the haptic device ($\sigma_{M_{\text{ext}}}, \bar{M}_{\text{ext}}$).

Operation efficiency was represented by the standard deviation of the UAV velocity and the elapsed time ($\sigma_{v_{\text{tot}}}, T_{el}$). Operator performance was expressed as the minimum distance between the waypoint location and the center of the UAV protection zone (D_{wp}). The level of safety was determined from the number of collisions and the minimum distance between the obstacle and the *boundary* of the UAV protection zone ($D_{\min}$).

The workload was measured after each run using the NASA TLX rating scale [32].

B. Hypotheses

Our first two hypotheses were based on results from earlier experiments [12,16].

1) Haptic feedback leads to a higher level of safety as compared with the condition without haptic feedback, expressed by a lower number of collisions and a larger distance to obstacles. This safety benefit is accompanied by, on average, a larger elapsed time.

2) Haptic feedback comes with an increase in operator subjective workload. That is, we expect that, despite the fact that the introduction of a time penalty will increase operators'

Table 2 Order of subtasks inside each sector used in the trajectories

	Subtask order
Sector 1	1-2-3-4-6-5
Sector 2	3-1-4-5-6-2
Sector 3	4-1-5-3-2-6

Table 3 Results of a full-factorial ANOVA of the main dependent measures, where ⋆⋆ and ⋆ represent chance levels of $p \leq 0.01$, $0.01, 0.01 < p < 0.05$, and $0.05 < p \leq 0.10$, respectively, and · indicates not significant.

Dependent measure	Control activity			Haptic activity		Minimum distance	UAV velocity	Elapsed time	Approach performance
	σ_{M_h}	$\bar{M}_h$	$\sigma_{\dot{\delta}_{\text{tot}}}$	$\sigma_{M_{\text{ext}}}$	$\bar{M}_{\text{ext}}$	$D_{\min}$	$\sigma_{v_{\text{tot}}}$	T_{el}	D_{wp}
Main effects									
CF	⋆⋆	⋆⋆	⋆⋆	⋆⋆	⋆⋆	⋆⋆	⋆⋆	⋆	⋆
ST	⋆⋆	⋆⋆	⋆⋆	⋆⋆	⋆⋆	⋆⋆	⋆⋆	·	·
Two-way interactions									
CF × ST	⋆⋆	⋆⋆	⋆⋆	⋆⋆	⋆⋆	⋆⋆	⋆⋆	⋆⋆	·

frustration level, the higher physical workload associated with haptic feedback is hypothesized to still dominate the final workload rating.

3) We hypothesized that workload will be lower with the force–stiffness feedback as compared with the force-feedback configuration. The force-feedback gains are smaller when stiffness is added, resulting in less variable neutral position changes. Control activity and haptic activity is hypothesized to be lower with the force–stiffness feedback.

4) The safety will further improve with the use of force–stiffness feedback, as operators more consistently yield to the guidance provided by the collision avoidance function.

VI. Results

Except when the total number of collisions is discussed, note that in the analysis of all other dependent measures only the runs *without* collisions were used.

A full-factorial within-subjects ANOVA was applied, using a Student–Newman–Keuls (SNK, $\alpha = 0.05$) post hoc analysis. Table 3 summarizes the ANOVA results. The number of collisions and the TLX workload ratings were analyzed using Kruskal–Wallis tests, followed by Mann–Whitney tests.

Figure 13 shows the number of collisions. The means and 95% confidence intervals of all other dependent measures are shown in Figs. 14 and 15. Here, the white, dark gray, and lighter gray bars represent the three control configurations NF, FF, and FSF, respectively. The numbers 1–6 on the horizontal axis correspond to the subtask numbers.

A. Objective Data

1. Number of Collisions

Figure 13 shows that, independent of the subtask, the number of collisions was largest without haptic feedback. A Kruskal–Wallis test revealed a highly significant effect of control configuration ($\chi^2 = 96.103$, $p \leq 0.01$). Force–stiffness feedback resulted in a significantly smaller number of collisions as compared with the condition with force feedback alone (Mann–Whitney, $Z = -2.058$, $p = 0.040$). These results are in support of hypotheses 1 and 4.

The figure further shows that subtask 5 resulted in by far the largest number of collisions (134), followed by subtasks 3 (63) and 6 (47). The smallest number of collisions occurred in subtasks 2 (15), 1 (18), and 4 (31), which were all expected to be relatively simple tasks.

In subtasks 3 and 5, both with closely spaced obstacles surrounding the UAV on both sides, the largest difference in the number of collisions was found between the conditions with and without haptic feedback. Particularly in subtask 5, the force–stiffness feedback resulted in a significantly smaller number of collisions than with the force-feedback condition (Mann–Whitney, $Z = -4.044$, $p \leq 0.01$); this subtask was reported by subjects to be the most difficult one. Note that here the potential for oscillatory stick motions to occur was largest, and apparently the stiffness feedback effectively reduced the chance of collisions, as expected. In all other subtasks, the differences between the two haptic configurations were minor.

2. Control Activity

The standard deviation of the total moment on the stick, exerted by the operator, σ_{M_h}, is shown in Fig. 14a. On average, σ_{M_h} was largest for the force–stiffness feedback conditions and smallest for the baseline condition, a highly significant effect (CF: $F_{2,20} = 24.454$, $p \leq 0.01$). Exceptions were subtasks 3 and 4, in which differences between control configurations were small, resulting in a highly significant two-way interaction (CF × ST: $F_{10,100} = 7.693$, $p \leq 0.01$). Regarding the dependency on the ST, subtask 2 resulted in the smallest moment variations, subtask 3 in the largest variations, resulting in a highly significant effect of subtask ($F_{5,50} = 19.619$, $p \leq 0.01$).

The mean of the moment exerted by the operator, $\bar{M}_h$, illustrated in Fig. 14b, was much higher for the two haptic feedback conditions, a highly significant effect (CF: $F_{2,20} = 72.398$, $p \leq 0.01$). Although the differences between the two haptic conditions were small, a post hoc analysis revealed that force–stiffness feedback resulted in the largest mean exerted moment. In subtask 3, the mean exerted moment was smallest, resulting in a highly significant effect of subtask ($F_{5,50} = 28.189$, $p \leq 0.01$). Here, the differences between haptic feedback and the baseline condition were much smaller, resulting in a significant two-way interaction (CF × ST: $F_{10,100} = 16.244$, $p \leq 0.01$).

Control activity in terms of the variations in the stick deflection rate, $\sigma_{\dot{\delta}_{\text{tot}}}$, shown in Fig. 14c, was lowest with the baseline condition and highest with the force-feedback condition, a highly significant effect (CF: $F_{2,20} = 8.558$, $p \leq 0.01$). In subtasks 1 and 4, with an

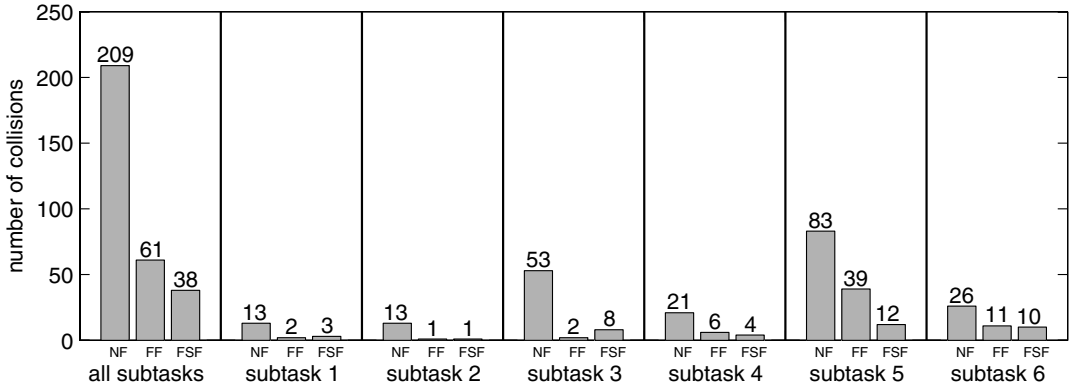

Fig. 13 Total number of collisions (all subjects).

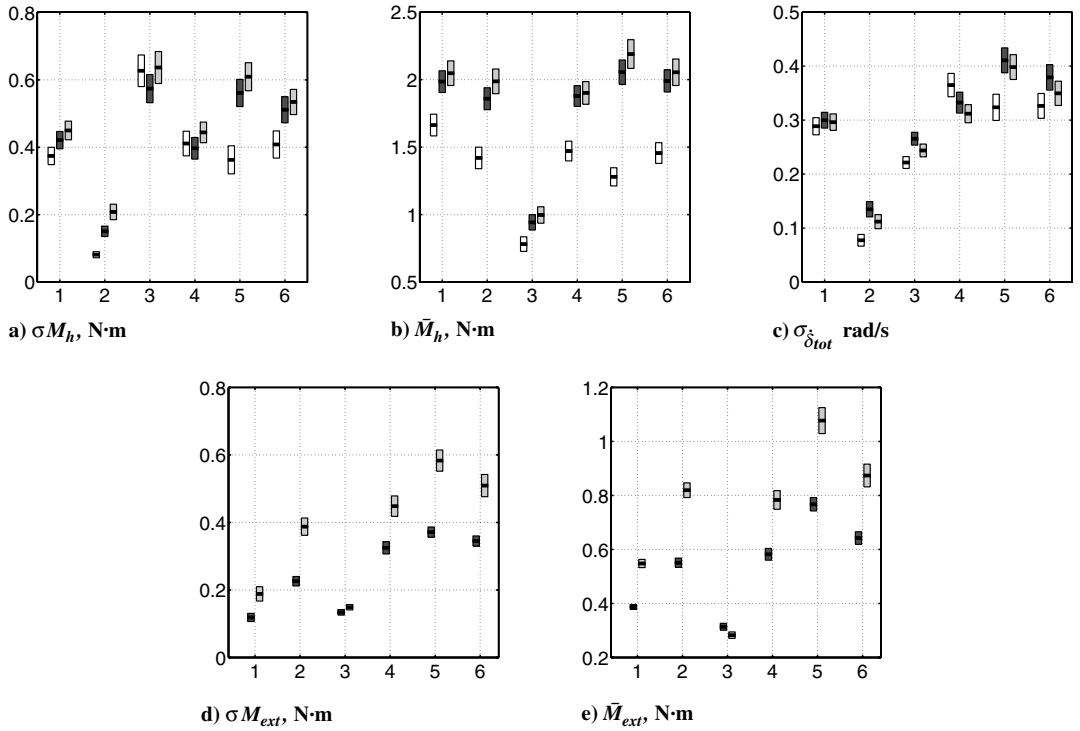

Fig. 14 Means and 95% confidence intervals of the control activity and haptic activity measures. The white, dark gray, and lighter gray bars represent the three control configurations NF, FF and FSF, respectively. Numbers 1–6 on the horizontal axis correspond to the subtask numbers. In d) and e), the basic configuration does not provide haptic feedback and is therefore not shown.

obstacle located at one side of the UAV, the baseline condition did not result in the smallest $\sigma_{\dot{\delta}_{tot}}$, however, resulting in a highly significant two-way interaction (CF × ST: $F_{10,100} = 9.082$, $p \leq 0.01$). In subtask 2, which required a relatively simple maneuver, $\sigma_{\dot{\delta}_{tot}}$ was smallest, whereas in subtask 5, involving a difficult approach and avoidance maneuver, $\sigma_{\dot{\delta}_{tot}}$ was largest, a highly significant subtask effect ($F_{5,50} = 29.251$, $p \leq 0.01$).

3. *Haptic Activity*

Here, obviously, the baseline condition was not considered. Figure 14d shows that, generally, the variations in the external moment, $\sigma_{M_{ext}}$, were largest with force–stiffness feedback, a highly significant effect (CF: $F_{1,10} = 53.909$, $p \leq 0.01$). In subtasks 1 and 3, the standard deviation of the external moment was smallest, whereas it was largest in subtask 5, a highly significant effect (ST: $F_{5,50} = 36.421$, $p \leq 0.01$). In subtask 3, the difference between force feedback and force–stiffness feedback was very small, resulting in a highly significant two-way interaction (CF × ST: $F_{5,50} = 11.573$, $p \leq 0.01$).

The mean external moment, $\bar{M}_{\text{ext}}$, illustrated in Fig. 14e, shows very similar trends. Overall, it was smallest with the force feedback (CF: $F_{1,10} = 90.891$, $p \leq 0.01$), except for subtask 3, in which it was smallest with the force–stiffness feedback (CF × ST: $F_{5,50} = 22.003$, $p \leq 0.01$), and it differed significantly for subtasks (smallest in subtask 3, largest in subtask 5; ST: $F_{5,50} = 45.818$, $p \leq 0.01$).

These results, and also those regarding control activity, do not support hypothesis 3.

4. *Minimum Distance*

The minimum distance, $D_{\min}$ (Fig. 15a) was largest with the haptic configurations, a highly significant effect (CF: $F_{2,20} = 72.091$, $p \leq 0.01$). Although the distance is, on average, smaller with the force–stiffness feedback, when compared with the force feedback alone, this difference was not significant (SNK, $\alpha = 0.05$). In subtask 3, the minimum distance was smallest, followed by subtask 5, which required a difficult maneuver and, indeed, resulted in the highest number of collisions. Subtask 1 resulted in the largest minimum distance, followed by subtask 4; both subtasks had an obstacle at only one side of the UAV (ST: $F_{5,50} = 28.026$, $p \leq 0.01$). In subtask 1, no differences between the control configurations were found at all, resulting in a highly significant two-way interaction (CF × ST: $F_{10,100} = 10.404$, $p \leq 0.01$). These results are in line with hypothesis 1.

5. *UAV Velocity*

The standard deviation of the total UAV velocity, $\sigma_{v_{tot}}$, shown in Fig. 15b, was smallest without haptic feedback, a highly significant effect (CF: $F_{2,20} = 14.287$, $p \leq 0.01$). Subtask 2 resulted in the smallest velocity variations and subtask 3 in the largest variations, which was expected as here the UAV had to move backward toward a building; hence, the subtask resulted in a highly significant effect ($F_{5,50} = 48.567$, $p \leq 0.01$). A post hoc analysis revealed the largest velocity variations with force–stiffness feedback, but only for subtasks 2 and 4, resulting in a highly significant two-way interaction (CF × ST: $F_{10,100} = 4.857$, $p \leq 0.01$).

6. *Elapsed Time*

The elapsed time, T_{el}, with no haptic feedback was significantly smaller than with haptic feedback (CF: $F_{2,20} = 5.391$, $p = 0.013$); see Fig. 15c. Recall that the situations in which collisions occurred were excluded from the analysis. For the elapsed time, no comparison was made between subtasks due to differences in trajectory length. However, a comparison of configurations within each subtask could still be done to investigate a possible two-way interaction. In subtasks 1, 2, 4, and 5, the elapsed time was smallest without haptic feedback, supporting hypothesis 1. In subtask 3, force–stiffness feedback resulted in the smallest elapsed time, which resulted in a highly significant two-way interaction (CF × ST: $F_{10,100} = 4.108$, $p \leq 0.01$). The visual information is very limited in subtask 3, as here the UAV is moving *backward* toward a building, and, unlike in the other subtasks, the operators almost completely relied on the haptic support.

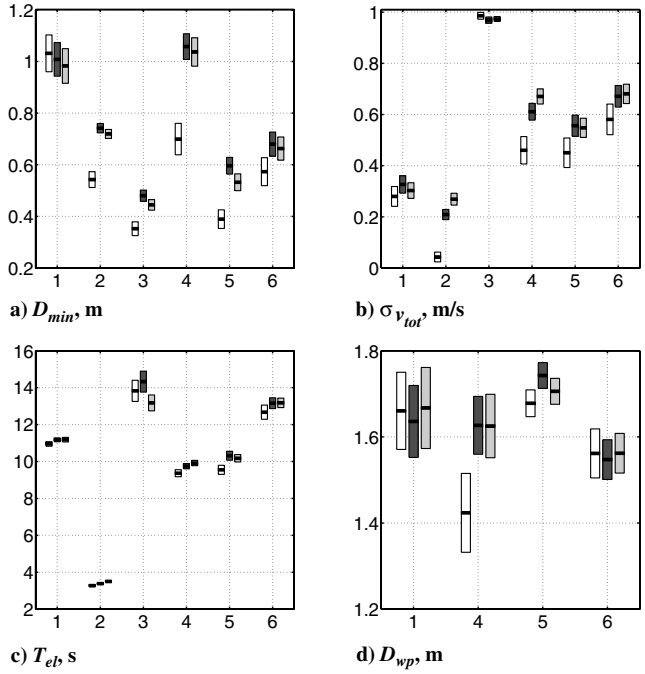

Fig. 15 Means and 95% confidence intervals of the safety, efficiency, and performance measures. The white, dark gray, and lighter gray bars represent the three control configurations NF, FF and FSF, respectively. Numbers 1–6 on the horizontal axis correspond to the subtask numbers. Subtasks 2 and 3 did not have smoke plumes serving as waypoints and are therefore not shown.

7. Approach Performance

When studying performance in terms of the minimum distance between the UAV and the waypoint, D_{wp}, subtasks 2 and 3 were not considered, because here the smoke only served as "noise" in the visual information of the obstacle boundaries rather than as a waypoint. Figure 15d shows that, on average, the distance was the same for all control configurations. Hence, the UAV passed the waypoints at equal distances for all control configurations and all subtasks, indicating that the subjects' interpretation of their task was the same for all conditions. The only exception occurs in subtask 4; here, the distance was smaller without haptic feedback, resulting in a significant control configuration effect ($F_{2,20} = 3.765,\ p = 0.041$). Note that many more collisions indeed occurred than with haptic feedback; see Sec. VI.A.1.

B. Subjective Data

1. Total Workload

Workload was measured after a whole run and can therefore not be analyzed for each individual subtask. Figure 16a shows the TLX rating of the total workload. In contrast to the findings in earlier experiments, the operators rated their workload to be the lowest with haptic feedback, a significant effect ($\chi^2 = 14.248,\ p \leq 0.01$). No significant difference was found between the force-feedback and force–stiffness feedback conditions. Hypotheses 2 and 3 must therefore both be rejected.

2. Sources for Workload

In the NASA TLX, operator workload consists of six sources: mental load (ML), physical load, temporal load, performance (PE), effort (EF), and frustration level (FL).

Figure 16 shows that haptic feedback resulted in the lowest mental load, a better judgment of own performance, and lower effort and frustration levels, all significant effects (ML: $\chi^2 = 25.863$, $p \leq 0.01$; PE: $\chi^2 = 27.455, p \leq 0.01$; EF: $\chi^2 = 10.299, p \leq 0.01$; FL: $\chi^2 = 26.783,\ p \leq 0.01$). As was expected, the baseline condition resulted in the lowest physical load ($\chi^2 = 28.574,\ p \leq 0.01$). Introducing the time penalty in the present experiment led subjects to weigh other causes for workload over the physical load. No significant differences between force feedback and force–stiffness feedback were found.

VII. Discussion

In our previous research on teleoperating a UAV in the presence of communication delays, it was found that haptic feedback (using force offset alone) resulted in higher levels of safety, but at the cost, however, of increased workload [16,30]. The goal of the current investigation was to improve haptic feedback using a novel force–stiffness combination.

The higher workload with conventional force feedback was hypothesized to be due to the physical workload associated with the feedback forces. Reducing the haptic feedback, for instance, through decreasing the force-feedback gain, could result in insufficient feedback for the collision avoidance function to be effective. The theoretical analysis, using offline computer simulations with a model of a typical operator's neuromuscular system, showed that a reduction of force feedback alone indeed leads to insufficient guidance information to avoid collisions. The combination of force feedback with an increased stiffness restored the collision avoidance performance. With force–stiffness feedback, the operator is forced to more consistently yield to the force-feedback command when close to an obstacle, and the increased stiffness also yields improved stability and less control signal oscillations [20], as can be concluded from the model analysis.

Human-in-the-loop experimental data show that, although control activity increased with haptic feedback, the number of collisions and operator workload *both* decreased significantly with respect to the baseline condition. Approach performance and efficiency, measured by the elapsed time and variations in velocity, also decreased with haptic feedback. However, these reductions were small in comparison with the significant increase in safety. The force–stiffness feedback did not significantly reduce operator workload with respect

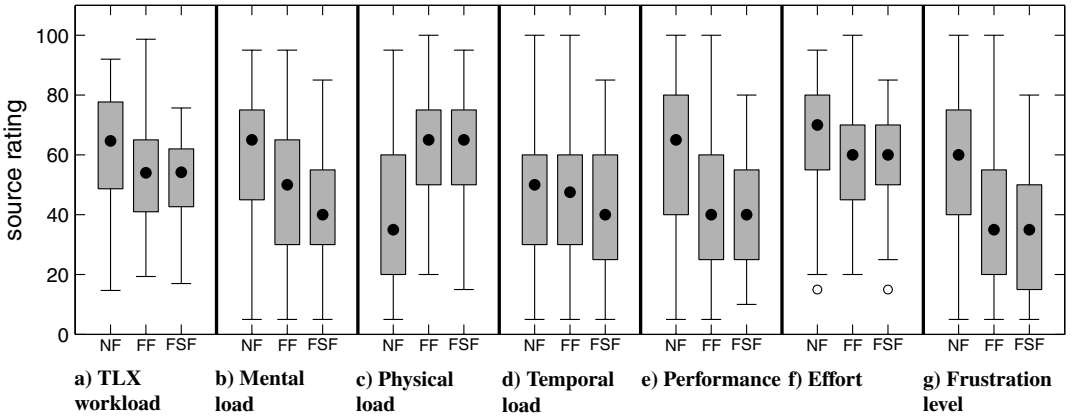

Fig. 16 Medians and interquartile ranges of TLX workload, including sources, with medium outliers (circles).

to the force-feedback condition; control activity and haptic activity did *not* reduce with force–stiffness feedback. It did result, however, in a significantly smaller number of collisions with equivalent workload when compared with force feedback alone.

The decrease in workload with respect to the "no haptic feedback" condition is in sharp contrast to the findings in previous research, in which workload was always rated highest with haptic feedback [12,16,19]. In those studies, no penalties or even indications were given, however, to subjects in the case of a collision. In the current experiment, each collision caused a penalty freeze of 60 s; this made subjects much more aware of their performance in all conditions and, in particular, in the situations without haptic feedback, as in those cases the number of collisions was relatively large. Because of the limited camera field of view, typical for many UAV teleoperation tasks, the operator in some cases, for example, when making a sharp turn around a corner, simply could not *see* whether a collision occurred or not. Thus, although physical load was rated lower without haptic feedback, as was expected, subjects apparently became more frustrated about their lack of performance and the high number of collisions. And as a result, they became more appreciative of the haptic feedback, as it helped them to significantly improve their collision avoidance performance, and they took the extra physical activity in stride. This result stresses the importance of creating realistic test conditions when using subjective workload ratings, such as the NASA TLX scale used in this study.

Although the force gain in the force–stiffness feedback was reduced, with the aim to decrease workload with respect to force feedback, experimental results did not yield a workload reduction. This could be attributed to the large variations and higher average of the external moment when flying with the force–stiffness feedback. The level of safety still further increased, however. The large external moments and variations of the force–stiffness feedback with respect to the force feedback offers the possibility of searching for a further reduction of the force–stiffness-feedback gains. It is very likely, however, that a tradeoff must be made between safety and workload. In that case, this study indicates that it might be more relevant to aim for higher levels of safety with the same workload, than to search for settings that yield lower workload with the same level of safety.

Additionally, it should be noted that the results also showed that, in spite of the larger repulsive moments produced by force–stiffness feedback, workload did not increase with respect to force feedback alone. Note that, although the repulsive moments were larger, the variations in the stick deflection *rate* were lower with respect to force feedback. Hence, variations in stick motions, particularly during difficult maneuvers between closely spaced obstacles, may contribute more to workload than the repulsive force amplitudes themselves.

The use of force–stiffness feedback in UAV teleoperation with time delays offers more potential to reduce operator workload than using force feedback alone. A compromise must be found between the gains of the force feedback and the stiffness feedback, and our first recommendation would be to search for better tuning settings. A second recommendation is to explore the benefits of using other variables to feed back through the control device's stiffness. In this study, *both* the force feedback as well as the stiffness feedback where coupled to the same artificial force field. It could well be that the stiffness feedback can be used to communicate other environmental variables to the human teleoperator, such as the relative distance to an obstacle, offering another degree of freedom in optimizing the haptic system.

Relatively straightforward adaptations to the stick for providing haptic feedback were considered here: an additional force and an increasing stiffness. One could also consider nonlinear adaptations with, for example, the application of different force gradients in the stick.

VIII. Conclusions

Haptic feedback was found to significantly increase the safety of teleoperating a UAV with time delays typical of a satellite communications link. In contrast to previous studies, subjective workload decreased with haptic feedback. Even though the haptic feedback conditions resulted in the highest physical load, subjects accepted this load, as the feedback allowed them to considerably improve their performance, reducing frustration, effort, and mental load.

With force–stiffness feedback, subjects are forced to yield more to the haptic feedback command, improving their performance in terms of safety, as compared with the situation with force feedback alone.

Although the current setting of the force–stiffness feedback allowed for smaller force-feedback gains, it did not result in a lower workload compared with force feedback alone. The force–stiffness feedback is a relatively simple design, and its tuning requires only two parameters, the design stiffness of the neuromuscular system and the stiffness gain. It was only evaluated for one combination of force offset gain and stiffness gain; it is recommended to further tune the feedback gains and explore other ways to manipulate the stiffness feedback, for example, by introducing nonlinear haptic feedback.

Acknowledgment

The authors thank the Netherlands Agency for Aerospace Programmes (NIVR) for their financial support of this project (NIVR project 49307TU).

References

[1] Sheridan, T. B., and Ferrell, W. R., "Remote Manipulative Control with Transmission Delay," *IEEE Transactions on Human Factors in Electronics*, Vol. HFE-4, No. 1, Sept. 1963, pp. 25–29. doi:10.1109/THFE.1963.231283

[2] Sheridan, T. B., "Space Teleoperation Through Time Delay: Review and Prognosis," *IEEE Transactions on Robotics and Automation*, Vol. 9, Oct. 1993, pp. 592–606. doi:10.1109/70.258052

[3] Monson, C. B., Fong, C. S., Marsh, R. A., and Haas, M. W., "Addressing the Human Element in Umanned Aerial Vehicles," *36th Aerospace Sciences Meeting & Exhibit*, AIAA, Washington, D.C., Jan. 1998, pp. 1–7; also AIAA Paper 98-1032.

[4] McCarley, J. S., and Wickens, C. D., "Human Factors Implications of UAVs in the National Airspace," Aviation Human Factors Division, Tech. Rept. AHFD-05-05/FAA-05-01, Savoy, IL, 2005.

[5] Lee, S., Sukhatme, G. S., Kim, G. J., and Park, C., "Haptic Control of a Mobile Robot: A User Study," *Proceedings of the 2002 IEEE/RSJ Intl. Conference on Intelligence Robots and Systems*, Vol. 3, Inst. of Electrical and Electronics Engineers, New York, 2002, pp. 2867–2874.

[6] Lim, J., Ko, J., and Lee, J., "Internet-Based Teleoperation of a Mobile Robot with Force-reflection," *Proceedings of 2003 IEEE Conference on Control Applications*, Vol. 1, Inst. of Electrical and Electronics Engineers, New York, June 2003, pp. 680–685.

[7] Xiao, D., and Hubbold, R., "Navigation Guided by Artificial Force Fields," *Proceedings of Conference on Human Factors in Computer Systems*, Addison Wesley, New York, April 1998, pp. 179–186.

[8] Elhajj, I., Xi, N., Fung, W. K., Liu, Y. H., Li, W. J., Kaga, T., and Fukuda, T., "Haptic Information in Internet-Based Teleoperation," *IEEE/ASME Transactions on Mechatronics*, Vol. 6, No. 3, Sept. 2001, pp. 295–304. doi:10.1109/3516.951367

[9] Repperger, D. W., Chandler, A. P., and Chelette, T. L., "A Study on Spatially Induced Virtual Force with an Information Theoretic Investigation of Human Performance," *IEEE Transactions on Systems, Man, and Cybernetics*, Vol. 25, No. 10, Oct. 1995, pp. 1392–1404. doi:10.1109/21.464442

[10] Repperger, D. W., Phillips, C. A., and Washington, K. R., "A Study on Stable Teleoperation with Time Delays and Haptic Interfaces," *Proceedings of the Ninth IFAC/IFIP/IFORS/IEA Symposium on Analysis, Design and Evaluation of Man-Machine Systems*, Georgia Inst. of Technology, Atlanta, Sept. 2004.

[11] Hannaford, B., Wood, L. P., McAffee, D. A., and Zak, H., "Performance Evaluated of a Six-Axis Generalized Force-Reflecting Teleoperator," *IEEE Transactions on Systems, Man, and Cybernetics*, Vol. 21, No. 3, May/June 1991, pp. 620–633. doi:10.1109/21.97455

[12] Lam, T. M., Mulder, M., and Van Paassen, M. M., "Haptic Interface for UAV Collision Avoidance," *International Journal of Aviation Psychology*, Vol. 17, No. 2, April 2007, pp. 167–195.

[13] Boschloo, H. W., Lam, T. M., Mulder, M., and Van Paassen, M. M., "Collision Avoidance for a Remotely-Operated Helicopter Using Haptic Feedback," *IEEE International Conference on Systems, Man and Cybernetics*, Inst. of Electrical and Electronics Engineers, New York, Oct. 2004, pp. 229–235.

[14] Anderson, R. J., and Spong, M. W., "Bilateral Control of Teleoperators with Time Delay," *IEEE Transactions on Automatic Control*, Vol. 34, No. 5, May 1989, pp. 494–501. doi:10.1109/9.24201

[15] Tanner, N. A., and Niemeyer, G., "Online Tuning ofWave Impedance in Telerobotics," *Proc. of IEEE Conference on Robotics, Automation, and Mechatronics*, Inst. of Electrical and Electronics Engineers, New York, Dec. 2004, pp. 7–12.

[16] Lam, T. M., Mulder, M., and Van Paassen, M. M., "Haptic Feedback in UAV Tele-Operation with Time Delay," *Journal of Guidance, Control, and Dynamics*, Vol. 31, No. 6, 2008, pp. 1728–1739. doi:10.2514/1.35340

[17] Niemeyer, G., and Slotine, J. J. E., "Stable Adaptive Teleoperation," *IEEE Journal of Oceanic Engineering*, Vol. 16, No. 1, Jan. 1991, pp. 152–162. doi:10.1109/48.64895

[18] Niemeyer, G., and Slotine, J. J. E., "Telemanipulation with Time Delays," *The International Journal of Robotics Research*, Vol. 23, No. 9, Sept. 2004, pp. 873–890. doi:10.1177/0278364904045563

[19] Lam, T. M., Mulder, M., and Van Paassen, M. M., "Haptic Feedback for UAV Tele-operation - Force Offset and Spring Load Modification," *IEEE International Conference on Systems, Man and Cybernetics*, Inst. of Electrical and Electronics Engineers, New York, Oct. 2006, pp. 1618–1623.

[20] Abbink, D. A., and Mulder, M., "Exploring the Dimensions of Haptic Feedback Support in Manual Control," *Journal of Computing and Information Science in Engineering* (to be published).

[21] Mulder, M., Abbink, D. A., and Boer, E. R., "The Effect of Haptic Guidance on Curve Negotiation Behavior of Young, Experienced Drivers," *Proceedings of the IEEE Conference on Systems, Man, & Cybernetics (IEEE—SMC)*, Inst. of Electrical and Electronics Engineers, New York, Oct. 2008.

[22] Schouten, A. C., "Proprioceptive Reflexes and Neurological Disorders," Ph.D. Dissertation, Faculty of Design, Engineering, and Production, Delft University of Technology, 2004.

[23] De Vlugt, E., "Identification of Spinal Reflexes," Ph.D. dissertation, Faculty of Design, Engineering, and Production, Delft University of Technology, Delft, The Netherlands, 2004.

[24] Lasschuit, J., "Modeling the Neuromuscular System Dynamics for Haptic Interface Design," M.Sc. Thesis, Faculty of Aerospace Engineering, Delft University of Technology, Delft, The Netherlands, 2007.

[25] Lam, T. M., D'Amelio, V., Mulder, M., and Van Paassen, M. M., "UAV Tele-Operation Using Haptics with a Degraded Visual Interface," *IEEE International Conference on Systems, Man and Cybernetics*, Inst. of Electrical and Electronics Engineers, New York, Oct. 2006, pp. 2440–2445.

[26] Olney, S. J., and Winter, D. A., "Predictions of Knee and Ankle Moments of Force in Walking from EMG and Kinematic Data," *Journal of Biomechanics*, Vol. 18, No. 1, 1985, pp. 9–20. doi:10.1016/0021-9290(85)90041-7

[27] Bobet, J., and Norman, R. W., "Least-Squares Identification of the Dynamic Relation Between the Electromyogram and Joint Moment," *Journal of Biomechanics*, Vol. 23, No. 12, 1990, pp. 1275–1276. doi:10.1016/0021-9290(90)90386-H

[28] Voorsluijs, G. M., Bennani, S., and Scherer, C. W., "Linear and Parameter-Dependent Robust Control Techniques Applied to a Helicopter UAV," *38th AIAA Guidance, Navigation and Control Conference*, AIAA, Reston, VA, Aug. 2004, pp. 1–11; also AIAA Paper 2004-4909.

[29] Lam, T. M., Boschloo, H. W., Mulder, M., and Van Paassen, M. M., "Artificial Force Field for Collision Avoidance in the UAV Tele-Operation," *IEEE Transactions on Systems, Man and Cybernetics. Part A* (to be published).

[30] Lam, T. M., Mulder, M., and Van Paassen, M. M., "Collision Avoidance in UAV Tele-Operation with Time Delay," *IEEE International Conference on Systems, Man and Cybernetics*, Inst. of Electrical and Electronics Engineers, New York, Oct. 2007, pp. 997–1002.

[31] McRuer, D. T., and Jex, H. R., "A Review of Quasi-Linear Pilot Models," *IEEE Transactions on Human Factors in Electronics*, Vol. HFE-8, No. 3, Sept. 1967, pp. 231–249.

[32] Hart, S. G., and Staveland, L. E., "Development of NASA-TLX (Task Load Index): Results of Empirical and Theoretical Research," *Human Mental Workload*, edited by P. A. Hancock and N. Meshkati, Elsevier Science Publishers, New York/Amsterdam, 1988, pp. 139–183.